Zero-Bias Anti-Ohmic Behaviour in Diradicaloid Molecular Wires

Amit Sil,[a,#] Lewis Hamilton,[b,#] James M. F. Morris,[a] Abdalghani H. S. Daaoub,[b] James H. H. Burrows,[a] Simon J. Higgins,[a] Hatef Sadeghi,[b] Richard J. Nichols,[a] Sara Sangtarash[b,*] & Andrea Vezzoli [a,*]

a) Department of Chemistry, University of Liverpool, Crown Street, Liverpool L69 7ZD, UK

b) Device Modelling Group, School of Engineering, University of Warwick, Coventry CV4 7AL, United Kingdom

# These authors contributed equally to this study

* Corresponding authors: andrea.vezzoli@liverpool.ac.uk

sara.sangtarash@warwick.ac.uk

Abstract

Open-shell materials bearing multiple spin centres hold the key to efficient charge transport in single-molecule electronic devices. They have very narrow bandgaps, and their partially occupied molecular orbitals align very efficiently to the Fermi level of the metallic electrodes of the single-molecule junction, thus allowing transparent electronic transport and higher conductance. Maintaining and stabilising multiple open-shell states, especially in contact with metallic electrodes is however very challenging, generally requiring a continuous chemical or electrochemical potential to avoid self-immolation of the open-shell character. To overcome this issue, we designed, synthesised, and measured the conductance of a series of bis(indeno) fused acenes, having a diradicaloid structure in resonance with a close-shell quinoidal conformation, providing steric protection with 3,5-dimethylthioanisole anchors to the electrodes and electronic protection against oxidation with tris(isopropyl)ethynyl substituents at the heart of the acene. We show here that these compounds have extremely anti-ohmic behaviour, with conductance *increasing* with increasing length at an unprecedented rate, across the entire bias window ($\pm\, 1.3\, V$). Density Functional Theory (DFT) calculations support our findings, showing the rapidly narrowing bandgap unique to these diradicaloid structures is responsible for the observed behaviour. Our results provide a framework for achieving efficient transport in neutral compounds and demonstrate the promise that diradicaloid materials have in single-molecule electronics, owing to their great stability and unique electronic structure.

Introduction

Open-shell materials (radicals) hold immense promise in many applications. They have unique magnetic and optoelectronic properties, which makes them ideal materials for organic spintronics[1] and organic photonics[2] and spearhead the next generation of molecular devices.[3] In the field of molecular electronics, organic radicals have been demonstrated to have enhanced charge transport efficiency[4,5] and Seebeck coefficient,[6–8] thanks to their low-lying molecular orbitals being more efficiently aligned with the Fermi level of the electrodes. Recently, it has been demonstrated that molecular wires bearing multiple spin centres (*e.g.* diradicals) behave like one-dimensional analogues of topological insulators,[9] granting long-range charge transport. Fabricating stable single-radical junction is however not trivial. Most studies rely on an external chemical[5,9] or electrochemical potential[10–12] to keep the molecular wire in its open-shell state, as self-immolation of the open-shell state[13] by charge transfer to/from the metallic electrodes is likely to occur at room temperature. In fact, while many open-shell molecular wires have been reported having retention of their radical nature at low temperature even in the absence of an external potential,[14,15] very few studies exist on the same happening at room temperature, and these are limited to exceptionally stable structures bearing a single radical state such as Kuhn's Verdazyls,[4] CF_3-stabilised Blatter radicals,[6] or fluorenyl species.[16]

Quinoidal polycyclic hydrocarbons are a uniquely tailorable source of open-shell materials.[17,18] In these materials an open-shell, diradicaloid aromatic structure is in resonance with its close-shell quinoidal counterpart. Depending on the degree of aromaticity and the number of π-sextets available the diradicaloid character y can be tuned, with $y = 1$ representing pure diradical behaviour.[19] Particularly attractive in these materials is that the synthetic process is relatively mild, with only a late-stage oxidation or reduction step delivering the reactive open-shell species, thereby allowing large freedom in designing the synthetic pathway. Bench stability is generally imparted by steric protection, decorating the edges of the polycyclic hydrocarbon with bulky *t*-butyl or mesityl substituents, thereby reducing the chance of dimerization or decomposition.

In this contribution, we show that diradicaloid species base on the (di)indenoacene family can be used to fabricate single-molecule junctions, showing outstanding properties. The diradicaloid character is tuned by the size of the acenyl core, and the efficiency of charge transport across the molecular wires *increases* as the molecule is made longer, resulting in a *negative* conductance attenuation β. Most

importantly, the negative β is consistent across the entire bias spectrum, as opposed to materials characterised so far where negative values for β have only been observed at high bias voltages,[20–23] with generally rapid conductance decay with length at low biases. Driving our devices at $V > 1\ V$ allow us to achieve unprecedented values of beta in excess of $-1\ \text{Å}^{-1}$. Furthermore, the fabricated devices show highly nonlinear $I - V$ characteristics, a desirable technological property for the development of high-performance molecular circuits,[24,25] arising from transport resonance closely aligned to the Fermi level of the electrodes enabling a resonant transport regime at relatively mild biases.

Results and Discussion

We focussed our efforts on the design of compounds **R1-R3** (Figure 1a). In all three cases, we settled on 3,5-dimethylthioanisole termini as contacts to the metallic electrodes, necessary to fabricate single-molecule junctions (Figure 1b). The methyl groups twist the thioanisolyl rings out of the acene plane and breaks conjugation into the electrodes, thereby providing to both steric protection against dimerization and electronic protection against self-immolation upon junction fabrication. We also provided electronic stabilisation against oxidation to **R2** and **R3** by adding triisopropylsylilethynyl substituents on the naphthyl or antracenyl core. Reports in the literature highlight the greatly enhanced stability of such compounds compared to the bare acene[26,27] while also providing the steric bulk necessary to direct the synthesis towards the desired isomer. We computed the diradicaloid character y using the Thermally Assisted Occupation (TAO) implementation of DFT[28] to calculate the partial occupancy of the frontier natural orbitals, and then applied the method originally developed by Yamaguchi[29] which gives $y = 1 - \frac{2T}{1+T^2}$ where $T = \frac{n_{HONO} - n_{LUNO}}{2}$. While originally developed for unrestricted Hartree-Fock calculations, TAO-DFT has been shown to perform exceptionally well for such calculations in acenes.[30] Our calculations predict an increase in the value of y from ~ 0.15 (indicating a weak diradicaloid character) for **R1** to ~ 0.3 for **R2** and ~ 0.5 for **R3**, in consistency with literature on similar compounds.[26,31] The chosen compounds have therefore diradicaloid character increasing with the [n]acene size.

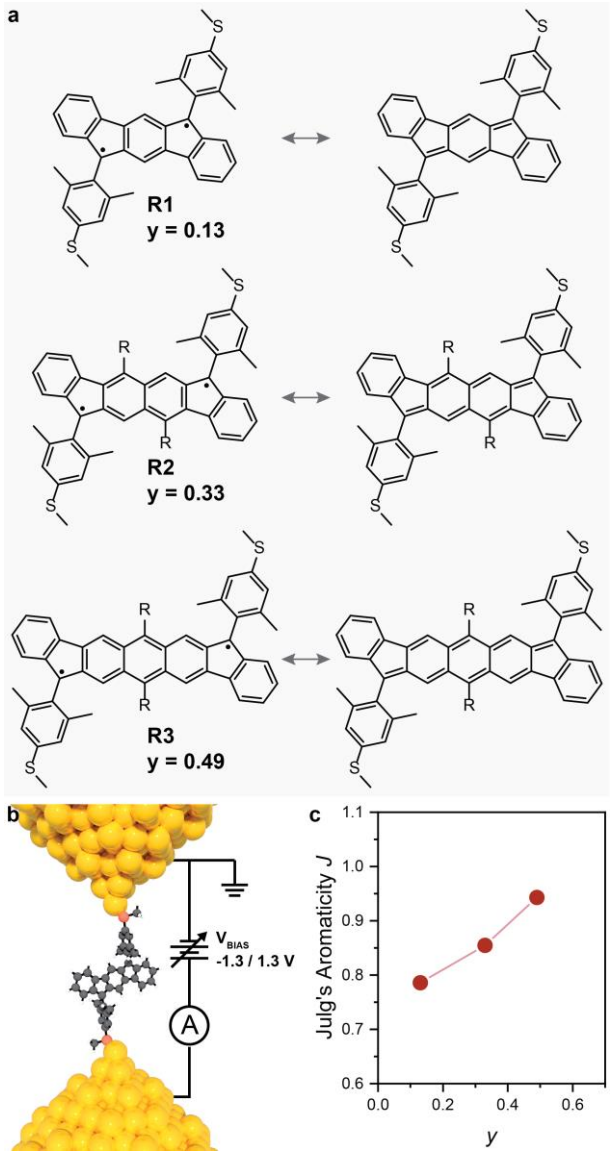

Figure 1: a) Structures of the molecular wires used in this study, in both their diradicaloid conformation and the quinoidal resonance structure. For **R2** and **R3**, R = tris(isopropyl)silylethynyl. The value of y expressed is calculated with TAO-DFT ($\theta = 22$), ULDA/6-31G* level of theory. b) Depiction of a single molecule junction fabricated with **R1**. c) Julg's aromaticity *vs* degree of diradicaloid character y.

We then proceeded to the synthesis of the three target compounds. Key in all three cases was the synthesis of the intermediate carbonyl compound, which was attained by series of Pd-catalysed Suzuki cross-coupling reactions. In the case of **R1**, the bis(carboxylic acid) ester was cyclised to the corresponding diketone with sulfuric acid and then treated with 4-lithio-3,5-dimethylthioanisole, followed by dehydration with stannous chloride. In the case of **R2** and **R3, t**he carbonyl compound was reacted with 4-lithio-3,5-dimethylthioanisole, cyclised with boron trifluoride etherate and then oxidised to the quinoidal/diradicaloid target compound with DDQ (2,3-dichloro-5,6-dicyano-1,4-benzoquinone). All compounds proved to be bench stable, and crystals suitable for X-ray diffraction studies could be grown

by vapour diffusion of pentane into concentrated acetonitrile solutions. Detailed synthetic procedures, characterisation and crystal structures can be found in the SI. The degree of diradicaloid character is clearly reflected in the crystal structures as an increase in Julg's aromaticity parameter J of the central arene/acene (benzene for **R1**, naphthalene for **R2**, anthracene for **R3**). The parameter can be calculated from the crystal structures as $J = 1 - \frac{225}{n}\sum_{i=1}^{n}\left(1 - {}^{d_n}/_{\bar{d}}\right)^2$, where d_n is each individual C-C bond length, and $\bar{d}$ is their mean value.[32] The less aromatic a system is, the lower is J, and for benzene (the archetypal purely aromatic system) $J = 1$. As a compound is more stable in its diradicaloid electronic configuration, the central unit acquires a more aromatic structure and the deviation of bond length from their mean value is reduced. Plotting Julg's aromaticity J *vs* y indeed shows a linear relationship (Figure 1c), highlighting the increasing destabilisation of the quinoidal resonance towards the aromatic diradicaloid structure across **R1-R3**.

We then used the scanning tunnelling microscope – break junction (STMBJ) technique to fabricate and characterise charge transport through single-molecule junctions fabricated with **R1-R3**. In this technique the STM z piezoelectric transducer is used to drive a Au tip into a Au-on-mica substrate under constant DC bias to fabricate a microcontact of conductance $G \gg G_0$, where G_0 is the conductance of an atomic point contact. The tip is then withdrawn at constant rate ($10\ nm\ s^{-1}$ in this study) to thin down the contact size to a single atom, having $G = G_0$, and rupture it to yield a pair of atomically sharp nanoelectrodes. The experiments are performed in the presence of the molecular wire of interest as a dilute solution in mesitylene, so that the single-molecule junction can self-assemble in the freshly formed nanogap through the formation of coordinative bonds between the aurophilic 3,5-dimethylthioanisole termini and the apical undercoordinated Au atoms on the two nanoelectrodes. As the junction is in place, we recorded the conductance *vs* electrode separation by continuing the withdrawal process until junction breakoff, under constant bias. The process is repeated thousands of times, and the results are analysed statistically in the form of histograms and density maps, to estimate the most probable conductance value (as G/G_0) and appreciate its distribution as a function of electrode separation.

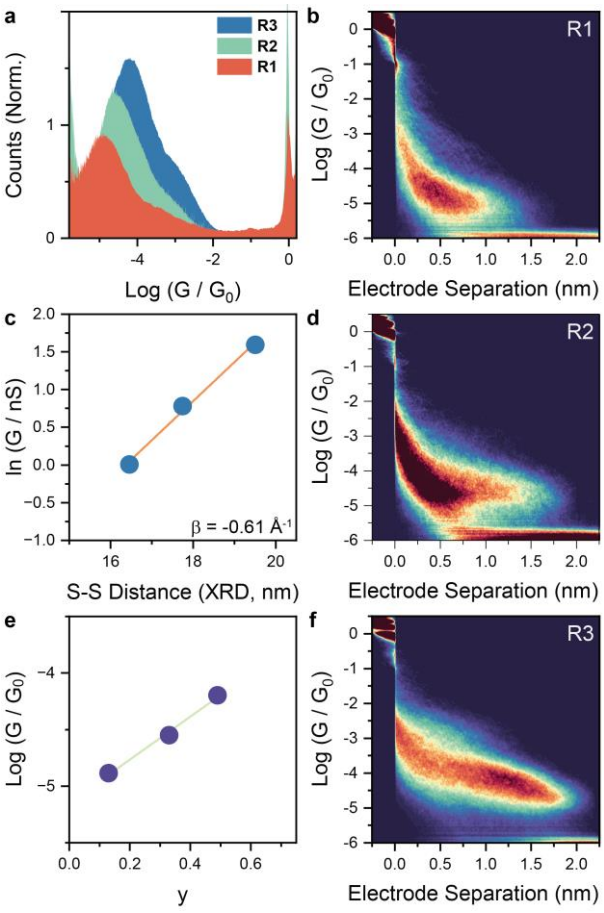

Figure 2: *STMBJ* Results. (a) Comparison of the single-molecule conductance histograms for **R1-R3**. (b) 2D conductance – electrode separation density map for **R1**. (c) Conductance attenuation plot for **R1-R3** showing a negative β factor of -0.61 Å^{-1}. (d) 2D conductance – electrode separation density map for **R2**. (e) Correlation between single-molecule conductance and degree of diradicaloid character y for **R1-R3**. (f) 2D conductance – electrode separation density map for **R3**. All *STMBJ* data acquired at 600 mV source-drain bias. All statistical plots compiled with 100 bins per conductance decade and 100 bins per nanometre. All experiments performed in freeze-pump-thawed mesitylene, with **R1-R3** at 1 mM concentration. No further effort were made at excluding oxygen from the STM liquid cell.

The results of our STMBJ investigations are reported in Figure 2. A continuous increase in conductance can be observed across the **R1-R3** series (Figure 2a), and the 2D density maps (Figure 2b,d,e) show that junctions can be stretched to increasing length, well commensurate with the S-S length of the corresponding molecular wire. Within the Landauer formalism based on a coherent tunnelling mechanism, the conductance G is expected to follow a logarithmic decay with conductance $G = Ae^{-\beta L}$, where the pre-exponential factor A is dependent on the chemical nature of the oligomeric series and L is the width of the tunnelling barrier. In our case, using the S-S distance determined by single-crystal X-Ray Diffraction (XRD) as L, we obtain a negative value of $\beta = -0.61\ \text{Å}^{-1}$, amongst the highest reported for single-molecule junctions at similar bias voltages. As first approximation, the negative conductance attenuation with length series can be rationalised through the increase in diradicaloid

character across the **R1-R3** series inferred from the TAO-DFT calculations discussed earlier. Plotting the single-molecule conductance *vs* the degree of diradicaloid character y returns an almost perfect semilogarithmic correlation, thereby suggesting that the degree of open-shell character is key in giving these materials their outstanding properties.

Performing measurements on **R3** at a lower source-drain bias, however, resulted in a lower conductance: Gaussian fits of the histogram peak are $10^{-4.7}G_0$ at 200 mV and $10^{-4.2}\ G_0$ at 600 mV (see SI for conductance histograms and 2D density maps). This large difference in conductance over a relatively mild increase in voltage suggest strong deviation from the low-bias Ohmic behaviour generally observed in molecular wires, which is a signature of resonant transport through a molecular orbital close in energy to the Fermi level of the electrodes.[33] Open-shell species, with their molecular orbitals being much better aligned to the Fermi level of the electrodes, are indeed ideal platforms for the study of these phenomena, and we have already reported evidence of nonlinear behaviour in a 6-oxoverdazyl derivative bearing a single spin centre.[4] We therefore acquired single-molecule $I-V$ characteristics of the junctions fabricated with **R1-R3**, using a modified *STMBJ* procedure. In this case, after formation of the metallic microcontact, the tip is withdrawn in a stepwise manner, with steps of height commensurate to the size of the junction evaluated in the corresponding 2D density map. Between steps, the source-drain bias is held at a constant value for 25 ms, then stepped and ramped between $\pm 1.3\ V$ over a period of 50 ms, and finally held constant again for further 25 ms. Data is then sliced and processed using the automated algorithms described in our previous publications where we used this technique.[4,34]

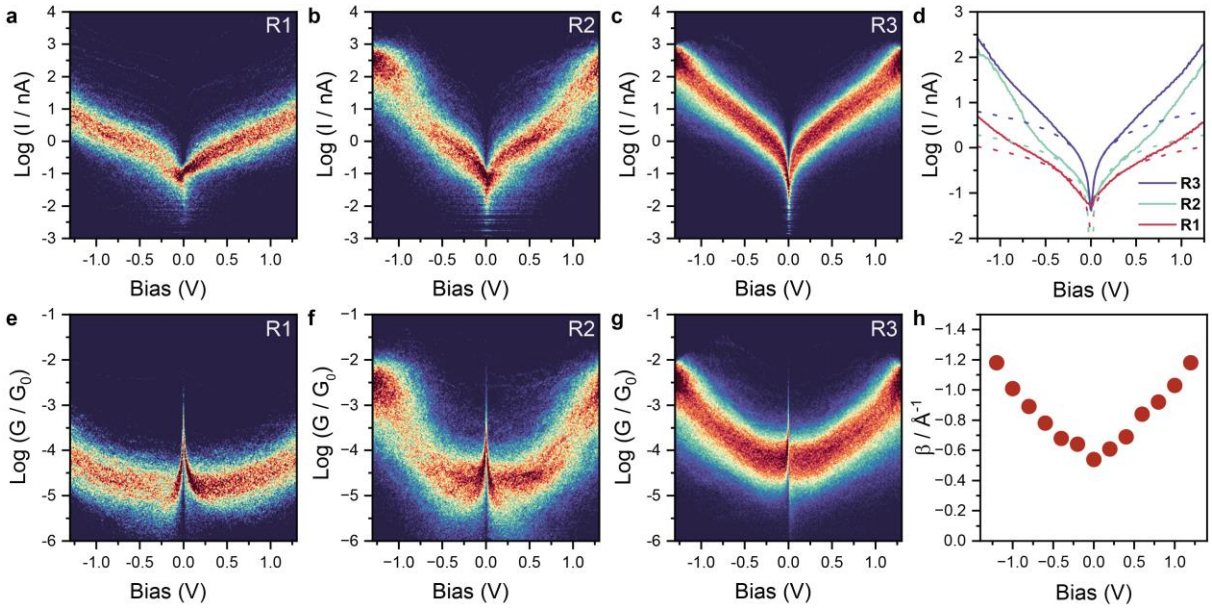

Figure 3: Single-molecule $I-V$ measurements. (a-c) $I-V$ density map for **R1-R3.** (d) Comparison between the Gaussian fittings of the $I-V$ density maps for the **R1-R3** series. The dashed lines correspond to the linear fitting of the low-bias regime ($\pm 100\ mV$). (e-f) $G-V$ density maps for **R1-R3**. (h) Conductance attenuation rate β *vs* bias V plot. All density maps compiled with 100 bins per decade and 100 bins per V. Data compiled from datasets consisting of 8672 (**R1**), 8454 (**R2**), and 10260 (**R3**) traces. The sharp feature at $V = 0$ in the $G-V$ curves is an artifact of our preamplifier due to low-bias currents being below the sensitivity of our instrumentation (bottom limit $\sim 20\ pA$).

The results of our $I-V$ investigations are reported in Figure 3. The behaviour observed in the static *STMBJ* measurements is found across the entire bias window, with current I consistently in the order $I_{R3} > I_{R2} > I_{R1}$ at each value of source-drain voltage. Gaussian fitting of individual vertical slices of the 2D maps (Figure 3a-c) enabled us to plot the comparison in Figure 3d. The low bias regime ($\pm\ 100\ mV$) was fitted to a linear Ohmic behaviour (dashed lines) to appreciate the increasing nonlinearity of these system and estimate the zero-bias value $\beta_0 = -0.54\ \text{Å}^{-1}$. Deviation from an Ohmic behaviour is observed at ~0.5 V for **R1**, ~0.3 V for **R2** and 0.1 V for **R3**, suggesting that a transport resonance becomes more closely aligned with the Fermi level of the electrodes as the bis(indeno)acene is made longer and its diradicaloid character y increases. This deviation from linear Ohmic behaviour is particularly evident in the $G-V$ maps (Figure 3e-g) which were used to calculate the dependence of the conductance attenuation factor β on source-drain bias. As can be observed in Figure 3h, the low-bias β of approximately $-0.6\ \text{Å}^{-1}$ increases to a remarkably high value of $-1.2\ \text{Å}^{-1}$ at 1.2 V bias.

To study quantum transport through the diradicaloids **R1-R3**, the ground state geometry was found using the SIESTA[35] implementation of Density Functional Theory (DFT). The frontier orbitals for each spin component of **R1-R3** were then calculated and plotted to identify spin-states and frontier orbital

patterns (more details in section 5 of the SI). Our results show identical spin-component orbital patterns and energy levels for **R1-R3,** with the wavefunctions delocalised over the entire polycyclic molecular backbone. The energy levels of the ground states of **R1-R3** configurations show a gradual narrowing of the HOMO-LUMO gap from 1.10 eV in **R1** by approximately 0.3 eV to a gap of 0.83 eV in **R2,** and even further to a gap of 0.62 eV in **R3**. It should be noted here that for **R2** and **R3** we performed our calculations with trimethylsilyl as acetylide termini rather than the experimentally synthesised tris(isopropyl)silyl derivatives to achieve higher computational efficiency. Given the low wavefunction density around the silyl units, this change is not expected to influence the behaviour of shifting energy levels. The ground state geometry used for orbital calculations gave us the baseline for attaching two pristine gold electrodes to SMe anchors of **R1-R3** and calculate the transmission probability $T(E)$ of electrons with energy E traversing from one electrode to the other using scattering theory.[36] Example scattering regions for **R2** and **R3** are shown in Figure 4a. Given the singlet ground state spin configuration of these material, all orbital spin-components show no polarization with the same ground state geometry, and the non-polarized DFT mean field Hamiltonian of each junction was combined with the transport code GOLLUM[37] to calculate $T(E)$.

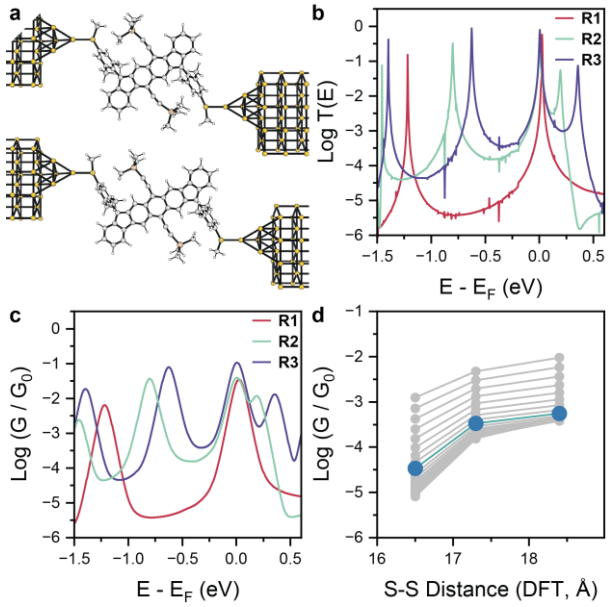

Figure 4: DFT Calculations. a) DFT-optimised configurations of **R2** and **R3** coordinated to the Au electrodes. b) Transmission coefficients $T(E)$ for **R1-R3**. c) Room-temperature conductance as a function of the DFT Fermi energy. d) Room-temperature conductance as a function of the DFT molecular length at likely Fermi energy ranges (divided evenly into 20 points between -0.4 eV and -0.2 eV). The energy that gives the closest agreement with the experimental data is highlighted in blue.

$T(E)$ results show a clear pinning of the DFT Fermi energy to the LUMO due to the choice of methyl thioether anchors (Figure 4b). With the LUMO pinned to E_F, the HOMO resonances for **R1-R3** shift to higher energies giving higher transmission for a wide energy range within the bandgap. Taking values at any position within the gap for **R3** (that has the smallest gap) shows an increase in T(E) from **R1** to **R3** and hence a negative beta factor. The change in bandgap width is larger between **R1/R2** compared to **R2/R3** in the orbital calculations (see section 5 of the SI), and this pattern is also reflected in our transmission curves. The rapid shrinking of the bandgap overcomes the natural tendency of molecular wire to display attenuated conductance with length,[38] leading to the observed increase of T(E). To demonstrate the effect of molecular length on electrical conductance, the room temperature conductance values for **R1-R3** were also calculated (Figure 4c). Measurements of S-S length using the ground state geometry was found be 16.5 Å, 17.3 Å and 18.3 Å for **R1-R3** respectively, in agreement with the lengths measured in the single-crystal XRD structure and the experimental STMBJ breakoff distances (see Figure 2). Using the calculated molecular length and conductance values, we plot the length dependence conductance for various Fermi energies within the HL gap (in the range -0.4 eV to -0.1 eV, see Figure 4d). The estimated ranges from $\beta = -0.88$ Å^{-1} for $E_F - 0.4\,eV$ to $\beta = -0.46$ Å^{-1} for $E_F = -0.1\,eV$. The best agreement with the zero-bias experimental value of $\beta = -0.54$ Å^{-1} is obtained at $E_F = -0.22\,eV$.

Conclusions

We demonstrated here that bis(indeno)acenes are a promising new scaffold in single-molecule electronics, allowing long-range efficient charge transport in single-molecule junctions. We synthesised three derivatives of increasing length, having indenofluorene (**R1**), fluorenofluorene (**R2**) and bis(indeno)anthracene (**R3**) structures. Single-molecule conductance was then measured using the STMBJ technique, and our results show increasing conductance with increasing length, with a clearly non-ohmic behaviour associated with a negative conductance attenuation factor $\beta = -0.6$ Å^{-1} at low bias. Single-molecule conductance appeared to be bias-dependent, and we therefore measured the single-molecule $I-V$ characteristics of these molecular wires, in the $\pm 1.3\,V$ bias window. Deviation from a low-bias ohmic behaviour was observed at decreasing bias, resulting in a bias-dependent attenuation factor reaching an unprecedented -1.2 Å^{-1} at $1.2\,V$ bias. In stark contrast with other systems that have been described in the literature having negative values of β, such as porphyrin

tapes[23] or cumulenes,[22] in this family of molecular wires the attenuation factor maintains its negative sign throughout the entire bias window of interest, with an extrapolated zero-bias value of $\beta = -0.54\ \text{Å}^{-1}$. These outstanding properties arise from their open-shell character, that creates a bandgap of decreasing size as the bis(indeno)acene is made longer, contributing to more efficient mid-bandgap transport. Most important, the open-shell state is inherent to the structure of the molecular wire, and it is not dependent on an external chemical or electrochemical potential to remain stable within the bias window of interest. These results show the promise that diradicaloid systems have in electronic applications, owing to their greatly tuneable bandgap and diradicaloid characters.

Methods

All synthetic procedures, details about the STMBJ technique and the instrumentation used in this study, and parameters for the DFT calculations, along with further extended data can be found in the Supplementary Information.

Acknowledgements

This work was supported by EPSRC (EP/V037765/1) and the Royal Society (RGS\R2\202119). AV thanks the Royal Society for a University Research Fellowship (URF\R1\191241). HS thanks UKRI for a Future Leaders Fellowship (MR/S015329/2 and MR/X015181/1). SS acknowledges the Leverhulme Trust for an Early Career Fellowship (ECF-2018-375).

Bibliography

1. Zhu, Y., Jiang, Q., Zhang, J. & Ma, Y. Recent Progress of Organic Semiconductor Materials in Spintronics. *Chemistry – An Asian Journal* **18**, e202201125 (2023).
2. Gorgon, S. *et al.* Reversible spin-optical interface in luminescent organic radicals. *Nature* **620**, 538–544 (2023).
3. Ji, L., Shi, J., Wei, J., Yu, T. & Huang, W. Air-Stable Organic Radicals: New-Generation Materials for Flexible Electronics? *Advanced Materials* **32**, 1908015 (2020).
4. Naghibi, S. *et al.* Redox-Addressable Single-Molecule Junctions Incorporating a Persistent Organic Radical. *Angewandte Chemie International Edition* **61**, e202116985 (2022).

5. Liu, J. *et al.* Radical-Enhanced Charge Transport in Single-Molecule Phenothiazine Electrical Junctions. *Angewandte Chemie International Edition* **56**, 13061–13065 (2017).
6. Hurtado-Gallego, J. *et al.* Thermoelectric Enhancement in Single Organic Radical Molecules. *Nano Letters* **22**, 948–953 (2022).
7. Sangtarash, S. & Sadeghi, H. Radical enhancement of molecular thermoelectric efficiency. *Nanoscale Advances* **2**, 1031–1035 (2020).
8. Alsaqer, M., Daaoub, A. H. S., Sangtarash, S. & Sadeghi, H. Large Mechanosensitive Thermoelectric Enhancement in Metallo-Organic Magnetic Molecules. *Nano Lett.* **23**, 10719–10724 (2023).
9. Li, L. *et al.* Highly conducting single-molecule topological insulators based on mono- and di-radical cations. *Nat. Chem.* **14**, 1061–1067 (2022).
10. O'Driscoll, L. J. *et al.* Electrochemical control of the single molecule conductance of a conjugated bis(pyrrolo)tetrathiafulvalene based molecular switch. *Chem. Sci.* **8**, 6123–6130 (2017).
11. Haiss, W. *et al.* Redox State Dependence of Single Molecule Conductivity. *Journal of the American Chemical Society* **125**, 15294–15295 (2003).
12. Osorio, H. M. *et al.* Electrochemical Single-Molecule Transistors with Optimized Gate Coupling. *Journal of the American Chemical Society* **137**, 14319–14328 (2015).
13. Low, J. Z. *et al.* The Environment-Dependent Behavior of the Blatter Radical at the Metal-Molecule Interface. *Nano Letters* **19**, 2543–2548 (2019).
14. Frisenda, R. *et al.* Kondo Effect in a Neutral and Stable All Organic Radical Single Molecule Break Junction. *Nano Letters* **15**, 3109–3114 (2015).
15. Hayakawa, R. *et al.* Large Magnetoresistance in Single-Radical Molecular Junctions. *Nano Letters* **16**, 4960–4967 (2016).
16. Yang, X. *et al.* Quasi-Free Electron States Responsible for Single-Molecule Conductance Enhancement in Stable Radical. *J. Phys. Chem. Lett.* **14**, 4004–4010 (2023).
17. Casado, J. Para-Quinodimethanes: A Unified Review of the Quinoidal-Versus-Aromatic Competition and its Implications. *Top Curr Chem (Z)* **375**, 73 (2017).
18. Casares, R. *et al.* Engineering the HOMO–LUMO gap of indeno[1,2- *b*]fluorene. *J. Mater. Chem. C* **10**, 11775–11782 (2022).

19. Kaur, P. & Ali, M. E. The influence of the radicaloid character of polyaromatic hydrocarbon couplers on magnetic exchange interactions. *Phys. Chem. Chem. Phys.* **24**, 13094–13101 (2022).
20. Li, L. *et al.* Topological Radical Pairs Produce Ultrahigh Conductance in Long Molecular Wires. *J. Am. Chem. Soc.* **145**, 2492–2498 (2023).
21. Garner, M. H., Bro-Jørgensen, W., Pedersen, P. D. & Solomon, G. C. Reverse Bond-Length Alternation in Cumulenes: Candidates for Increasing Electronic Transmission with Length. *The Journal of Physical Chemistry C* **122**, 26777–26789 (2018).
22. Xu, W. *et al.* Unusual Length Dependence of the Conductance in Cumulene Molecular Wires. *Angewandte Chemie International Edition* **58**, 8378–8382 (2019).
23. Leary, E. *et al.* Bias-Driven Conductance Increase with Length in Porphyrin Tapes. *Journal of the American Chemical Society* **140**, 12877–12883 (2018).
24. Greenwald, J. E. *et al.* Highly nonlinear transport across single-molecule junctions via destructive quantum interference. *Nature Nanotechnology* **16**, 313–317 (2021).
25. Tamaki, T. & Ogawa, T. Nonlinear and Nonsymmetric Single-Molecule Electronic Properties Towards Molecular Information Processing. *Topics in Current Chemistry* **375**, 79 (2017).
26. Rudebusch, G. E. *et al.* Diindeno-fusion of an anthracene as a design strategy for stable organic biradicals. *Nature Chem* **8**, 753–759 (2016).
27. Fudickar, W. & Linker, T. Why Triple Bonds Protect Acenes from Oxidation and Decomposition. *J. Am. Chem. Soc.* **134**, 15071–15082 (2012).
28. Chen, B.-J. & Chai, J.-D. TAO-DFT fictitious temperature made simple. *RSC Adv.* **12**, 12193–12210 (2022).
29. Yamaguchi, K., Okumura, M., Takada, K. & Yamanaka, S. Instability in chemical bonds. II. Theoretical studies of exchange-coupled open-shell systems. *International Journal of Quantum Chemistry* **48**, 501–515 (1993).
30. Chai, J.-D. Thermally-assisted-occupation density functional theory with generalized-gradient approximations. *The Journal of Chemical Physics* **140**, 18A521 (2014).
31. Xu, T. *et al.* Antiaromatic Dicyclopenta[b,g]/[a,f]naphthalene Isomers Showing an Open-Shell Singlet Ground State with Tunable Diradical Character. *J. Am. Chem. Soc.* **143**, 20562–20568 (2021).

32. Julg, A. & François, P. Recherches sur la géométrie de quelques hydrocarbures non-alternants: son influence sur les énergies de transition, une nouvelle définition de l'aromaticité. *Theoret. Chim. Acta* **8**, 249–259 (1967).
33. Zang, Y. *et al.* Resonant Transport in Single Diketopyrrolopyrrole Junctions. *Journal of the American Chemical Society* **140**, 13167–13170 (2018).
34. Wu, C. *et al.* A Chemically Soldered Polyoxometalate Single-Molecule Transistor. *Angewandte Chemie International Edition* **59**, 12029–12034 (2020).
35. Soler, J. M. *et al.* The SIESTA method for ab initio order- N materials simulation. *Journal of Physics: Condensed Matter* **14**, 2745–2779 (2002).
36. Sadeghi, H. Theory of electron, phonon and spin transport in nanoscale quantum devices. *Nanotechnology* **29**, 373001 (2018).
37. Ferrer, J. *et al.* GOLLUM: a next-generation simulation tool for electron, thermal and spin transport. *New Journal of Physics* **16**, 093029 (2014).
38. Algethami, N., Sadeghi, H., Sangtarash, S. & Lambert, C. J. The Conductance of Porphyrin-Based Molecular Nanowires Increases with Length. *Nano Lett.* **18**, 4482–4486 (2018).